AGU PUBLICATIONS

JGR

Journal of Geophysical Research: Solid Earth

RESEARCH ARTICLE

10.1002/2017JB014168

Key Points:
- The elasticity, moduli, and seismic velocities of epsilon-FeOOH were determined to 140 GPa using density functional theory
- Iron-rich solid solutions from the FeOOH–AlOOH–$MgSiH_2O_4$ system are plausible contributors to the seismic properties of the large low-shear velocity provinces
- Epsilon-FeOOH exhibits $S_H > S_V$ shear wave polarization anisotropy similar to what is seismically observed at the base of the lower mantle

Supporting Information:
- Supporting Information S1

Correspondence to:
E. C. Thompson,
ecthompson@uchicago.edu

Citation:
Thompson, E. C., A. J. Campbell, and J. Tsuchiya (2017), Elasticity of ε-FeOOH: Seismic implications for Earth's lower mantle, *J. Geophys. Res. Solid Earth*, *122*, doi:10.1002/2017JB014168.

Received 3 MAR 2017
Accepted 9 JUN 2017
Accepted article online 7 JUL 2017

Elasticity of ε-FeOOH: Seismic implications for Earth's lower mantle

E. C. Thompson[1], A. J. Campbell[1], and J. Tsuchiya[2]

[1]Department of the Geophysical Sciences, University of Chicago, Chicago, Illinois, USA, [2]Geodynamics Research Center, Ehime University, Matsuyama, Japan

Abstract We have calculated the structure and elasticity of low-spin ferromagnetic ε-FeOOH to 140 GPa using density functional theory calculations with a Coulombic self-interaction term (U). Using these data, the elastic moduli and sound velocities of ε-FeOOH were calculated across the pressure stability of the hydrogen bond symmetrized structure (30 to 140 GPa). The obtained values were compared with previously published values for phase H ($MgSiH_2O_4$) and δ-AlOOH, which likely form a solid solution with ε-FeOOH. In contrast to these Mg and Al end-members, ε-FeOOH has smaller diagonal and larger off-diagonal elastic constants, leading to an eventual negative pressure dependence of its shear wave velocity. Because of this behavior, iron-enriched solid solutions from this system have smaller shear wave velocities than surrounding mantle and therefore are a plausible contributor to large low-shear velocity provinces (LLSVPs) which exhibit similar seismic properties. Additionally, ε-FeOOH has substantial shear wave polarization anisotropy. Consequently, if iron-rich solid solutions from the FeOOH–AlOOH–$MgSiH_2O_4$ system at the core-mantle boundary exhibit significant lattice-preferred orientation due to the strong shear stresses which occur there, it may help explain the seismically observed $S_H > S_V$ anisotropy in this region.

1. Introduction

Even relatively small amounts of "water" (OH−) within the crystalline structure of deep Earth minerals profoundly influence the bulk properties of the minerals that contain it—influencing melting temperatures [e.g., *Inoue*, 1994], rheological behavior [e.g., *Karato et al*., 1986], and electrical conductivity [e.g., *Wang et al*., 2006]. Owing to the outsized influence of hydrous phases, even in relatively small volumes, on geophysical interpretations of the interior of Earth, there has been a recent surge of research investigating the budget, storage, and cycling of hydrogen in the Earth's mantle. Recent advances in experimental [e.g., *Bindi et al*., 2015] and computational [e.g., *Panero and Caracas*, 2017] techniques have aided these efforts. In particular, ab initio studies have played a leading role in understanding the properties and structures of hydrous phases at extreme conditions and have proven complementary to ongoing experimental efforts [e.g., *Tsuchiya*, 2013].

Goethite (α-FeOOH) is an abundant and widespread iron oxy-hydroxide found in sediments, ore deposits, and as a primary component of rust at the Earth's surface. This low-pressure structure undergoes a first-order phase transition accompanied by a 7% density increase, transforming into the high-pressure phase ε-FeOOH at ~6 GPa [*Bendeliani et al*., 1972; *Gleason et al*., 2008]. Structural refinement based on moderate-pressure (<10 GPa) X-ray and neutron diffraction experiments indicate that ε-FeOOH is orthorhombic (space group $P2_1nm$, $Z = 2$), composed of edge sharing FeO_6 units that are closely packed along the c axis, forming a rutile-like structure with hydrogen occupying the channels between the edge-sharing chains [e.g., *Bolotina et al*., 2008]. This high-pressure phase is reported to undergo a pressure-induced hydrogen bond symmetrization leading to a second-order phase transition from $P2_1nm$ to $Pnnm$, [e.g., *Gleason et al*., 2008]. The high-pressure symmetric phase is shown in Figure 1, as is the spin polarization density of the iron atoms within the structure. Unfortunately, the exact pressure of this hydrogen bond symmetrization has been difficult to assess, as the corresponding volume change is minimal and hydrogen's minimal cross section makes its position indeterminate by X-ray diffraction. Previously reported pressures of hydrogen bond symmetrization have ranged from 25 to 45 GPa [*Xu et al*., 2013; *Gleason et al*., 2013]. Additionally, ε-FeOOH has been experimentally demonstrated to undergo a spin transition between 40 and 60 GPa [*Gleason et al*., 2013]. There are numerous complications inherent to experiments on iron-bearing, hydrous phases, including the multiple valence states of iron, defects associated with hydrogen substitution, and in the case of X-ray diffraction studies, the need for a secondary probe to enable the detection of hydrogen [e.g., *Hu et al*., 2016]. These

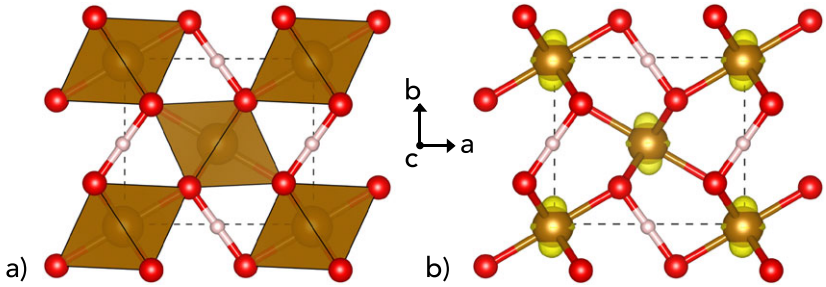

Figure 1. High-pressure hydrogen-centered (HC) ε-FeOOH structure. (a) Crystal structure at 30 GPa with orange polyhedral representing FeO_6. Large red spheres are O atoms and smaller white spheres are H atoms. (b) Spin polarization density map ($\rho_{up} - \rho_{down}$) at 30 GPa with yellow isosurface indicating a value of 0.078 $e^-/a.u.^3$. Both images were generated in VESTA [*Momma and Izumi*, 2008].

complications render phases such as FeOOH ideal candidates for study via density functional theory (DFT) calculations, particularly in determining material properties at the extreme pressures relevant to the Earth's mantle.

At ambient pressure, goethite (α-FeOOH) is isomorphous with the low-pressure aluminum oxide hydroxide diaspore (α-AlOOH). As with goethite, diaspore undergoes a pressure-induced phase change, transforming into the high-pressure phase δ-AlOOH, which is isostructural with the high-pressure phase ε-FeOOH [*Suzuki*, 2010]. As with ε-FeOOH, δ-AlOOH undergoes a second-order phase transition due to hydrogen bond symmetrization, though at slightly higher pressures [*Tsuchiya et al*., 2002; *Sano-Furukawa et al*., 2009; *Kuribayashi et al*., 2014]. It is presumable that the post hydrogen bond symmetrized structures of these compositions form a solid solution, which is particularly exciting as δ-AlOOH has a pressure–temperature (*P–T*) stability that extends to the Earth's core–mantle boundary (CMB) [*Sano et al*., 2008].

Recently a new dense hydrous magnesium silicate, phase H ($MgSiH_2O_4$), was predicted via DFT calculations and subsequently confirmed experimentally [*Tsuchiya*, 2013; *Ohtani et al*., 2014]. This phase has the highest reported *P-T* stability of any of the so-called "alphabet" phases of dense hydrous magnesium silicates. Phase H also belongs to the *Pnnm* space group [*Bindi et al*., 2014], and there likely exists a solid solution between phase H, δ-AlOOH, and ε-FeOOH. Aluminum substitution has been experimentally determined to stabilize phase H, but the precise influence of iron on this system remains poorly defined. This study aims to describe the high-pressure elasticity of low-spin hydrogen-symmetric ε-FeOOH, as a means of better understanding the stability and properties of the only known hydrous solid solution with *P-T* stability that extends throughout the Earth's mantle.

2. Methods

First principles calculations were conducted using the generalized gradient approximation (GGA) to the exchange-correlation functional [*Perdew et al*., 1996], as it has previously been found to better describe hydrogen bonding compared to a local density approximation (LDA) [e.g.; *Umemoto and Wentzcovitch*, 2005]. Density functional theory calculations were performed both with and without the addition of an on-site Coloumbic self-interaction term (*U*). The addition of a Hubbard *U* term is critical to accurately describe the stability, electronic, magnetic, and elastic properties of iron-bearing systems, as is the selection of an appropriate *U* value [e.g., *Jang et al*., 2017]. In the case of GGA + *U* calculations, Hubbard *U* values were determined by an internally consistent method [*Cococcioni and de Gironcoli*, 2005; *Tsuchiya et al*., 2006; *Nishi et al*., 2017], and a secondary set of calculations were performed with a fixed value of $U = 5$ to allow direct comparison with literature values [e.g., *Gleason et al*., 2008]. All values reported herein reflect self-consistent *U* value calculations unless otherwise indicated. Relaxed structures were solved using damped variable cell shape molecular dynamics [*Wentzcovitch*, 1991] as part of the Quantum ESPRESSO Package [*Giannozzi et al*., 2009]. The effective interaction of core electrons was approximated using previously evaluated norm-conserving pseudopotentials [*Troullier and Martins*, 1991] with the exception of iron, in which case ultrasoft pseudopotentials were employed [*Vanderbilt*, 1990; *Ichikawa et al*., 2014]. The irreducible Brillouin zone was sampled by a 4 × 4 × 8 Monkhorst-Pack mesh [*Monkhorst and Pack*, 1976] and electronic wave

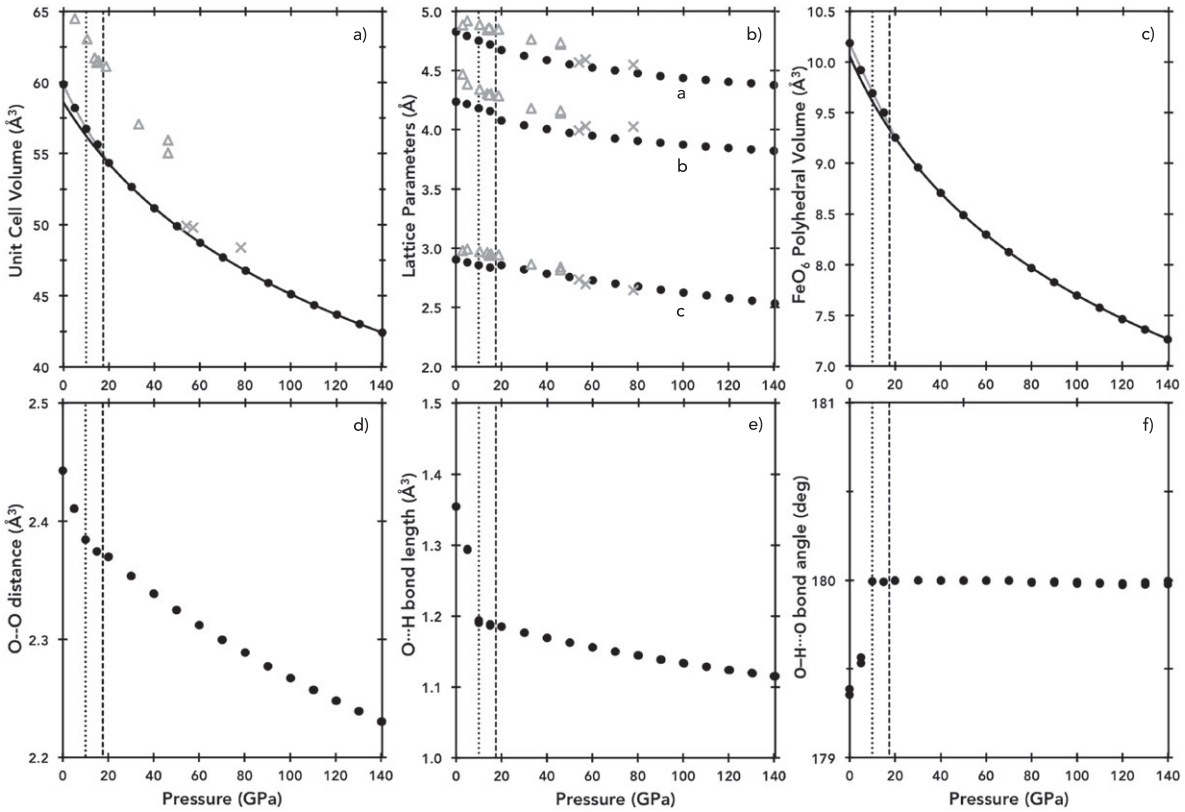

Figure 2. Calculated structural parameters of low-spin ferromagnetic ε-FeOOH from 0 to 140 GPa by GGA + U including (a) unit cell volume, (b) lattice parameters, (c) FeO_6 polyhedral volume, (d) O•••O distance, (e) O•••H bond length, (f) O–H•••O angle. Solid black lines are equations of state fitted to hydrogen-centered (HC) structures, while solid gray lines are equations of state fitted to hydrogen off-centered (HOC) low-pressure structures. Dotted line indicates pressure at which hydrogen bond symmetrization occurs, dashed line indicates pressure at which symmetry change occurs, and gray symbols are experimental data from *Gleason et al*. [2013], with open triangles indicating high-spin ε-FeOOH and crosses indicating low-spin ε-FeOOH.

functions were expanded in plane waves with an energy cutoff of 80 Ry. The effects of larger energy cutoffs and *k* point sampling were found to be negligible. Elastic constants were determined by applying strains of magnitude 0.01–0.001 depending on the linearity of stress-strain relations [*Karki et al*., 2001] to relaxed, static (0 K) structures.

3. Results and Discussion

3.1. Structure

Structural parameters of ε-FeOOH from the GGA + *U* calculations are plotted in Figure 2, and a tabulated version can be found in Table S1 in the supporting information. Analyses of the relaxed structural parameters based on both GGA and GGA + *U* calculations reveal a discontinuity consistent with a second-order phase transition due to hydrogen bond symmetrization at ~10 GPa. Hydrogen bond symmetrization occurs when the hydroxyl bond length ($r_{O–H}$) is equal to the hydrogen bond length ($r_{O\cdots H}$), therefore comprising half the total oxygen to oxygen distance ($r_{O\cdots O}$). The FeO_6 polyhedral volume before and after hydrogen bond symmetrization were fit to third-order Birch-Murnaghan equations of state (Table 1). These polyhedral equations of state parameters indicate a change in primary strain accommodation mechanism before and after hydrogen bond symmetrization, with hydrogen bonds accommodating more relative strain prior to symmetrization, as seen in Figure 2. This shift in strain accommodation is reflected in the pronounced change in pressure derivative of the bulk modulus of the FeO_6 (Table 1). This change in strain accommodation mechanism leads to structural changes in both unit cell volume and lattice parameters (Figures 2a and 2b), a phenomenon previously reported in the experimental study of the effect of hydrogen-bond symmetrization on the compressibility of δ-AlOOH by *Sano-Furukawa et al*. [2009].

Table 1. Third-Order Birch-Murnaghan Equation of State Parameters of FeO_6 Polyhedra in the Low-Pressure Hydrogen Off-Center (HOC) Structure and High-Pressure Hydrogen Bond Symmetrized Structure (HC) Based On Self-Consistent U-Value Calculations[a]

	HOC (0–20 GPa)	HC (30–140 GPa)
V_0 (Å^3)	10.18(1)	10.06(1)
K_0 (GPa)	205(10)	196(1)
K'_0	1.09(83)	4.79(1)

[a]Values in parentheses are uncertainties on the last digit.

Calculated low-spin ε-FeOOH lattice parameters are in good agreement with previously reported experimental values by *Gleason et al*. [2013] albeit with a slight underestimate of lattice parameters as shown in Figure 2. Note, the experimental data shown reflects both high-spin and low-spin ε-FeOOH, and agreement with our calculations is only expected at the highest-pressure data points, as the high → low spin transition is associated with a significant decrease in unit cell volumes. Additionally, it should be noted that Gleason and coauthors found that their experimental data were best fit to their DFT calculation for antiferromagnetic (AFM) low-spin ε-FeOOH using a fixed *U* value. In this study we reevaluated the stability of both AFM and ferromagnetic (FM) structures on the basis of calculated enthalpy, and determined the FM structure to be slightly more stable (~0.03 eV) at all pressure points based on calculations using both a fixed or self-consistent *U* parameter (Figure S1). Monoclinic distortion (i.e., deviation from orthorhombic lattice angles of 90°) remained minimal (<1°) throughout the entire pressure range investigated.

3.2. Equation of State and Density of State

Compressive behavior of the unit cell as a whole changes as a result of hydrogen bond symmetrization, consistent with prior studies of hydrous phases including δ-AlOOH and phase H [*Tsuchiya and Tsuchiya*, 2009; *Tsuchiya and Mookherjee*, 2015]. Hydrogen bond symmetrization led to a ~19% increase in the bulk modulus (K_0) and a ~22% reduction of its pressure derivative (K'_0) (Table 2). Due to changes in compressional behavior coincident with the second-order transition due to hydrogen bond symmetrization, structures before and after hydrogen bond symmetrization were treated as separate phases and used to derive separate sets of equation of state parameters. Calculated volumes of optimized structures of both GGA and GGA + *U* calculations were used to fit third-order Birch-Murnaghan equations of state [*Birch*, 1947]:

$$P(V) = \frac{3K_0}{2}\left[\left(\frac{V_0}{V}\right)^{\frac{7}{3}} - \left(\frac{V_0}{V}\right)^{\frac{5}{3}}\right]\left\{1 + \frac{3}{4}\left(K_0^{'} - 4\right)\left[\left(\frac{V_0}{V}\right)^{\frac{2}{3}} - 1\right]\right\}$$

in which K_0 is the bulk modulus at ambient pressure, K'_0 is the first pressure derivative of the bulk modulus, V_0 is the reference volume. Results from these fits are listed in Table 1; the GGA + *U* results should be preferred because the *U* term provides a more accurate characterization of the transition metal bonding. This resulted in significantly lower errors in comparison to fitting the entire pressure range with a single equation of state. The reference volume (V_0) was treated as a free parameter in the equation of state fitting.

The density of states (DOS) of ferromagnetic low-spin ε-FeOOH was determined from optimized structures at five GPa intervals below 20 GPa and at 10 GPa intervals up to 140 GPa. These densities of state, referenced to the Fermi level, indicate a clear and abrupt change in orbital structure before and after hydrogen bond symmetrization (Figure S2). Densities of state at all pressures in the 0 to 140 GPa range exhibit nonzero bandgaps indicative of insulator behavior, with increased bandwidths at higher pressures. There is a secondary and

Table 2. Birch-Murnaghan Equation of State Parameters for the Low-Pressure Hydrogen Off-Center Structure (HOC; 0–20 GPa) and High-Pressure Hydrogen Bond Symmetrized Structure (HC; 30–140 GPa) for Self-Consistent U-Value Calculations[a]

	HOC (0–20 GPa)	HC (30–140 GPa)
V_0 (Å^3)	57.43(7)	58.62(5)
K_0 (GPa)	188(4)	223(2)
K'_0	5.19(12)	4.07(3)

[a]Values in parentheses are uncertainties on the last digit.

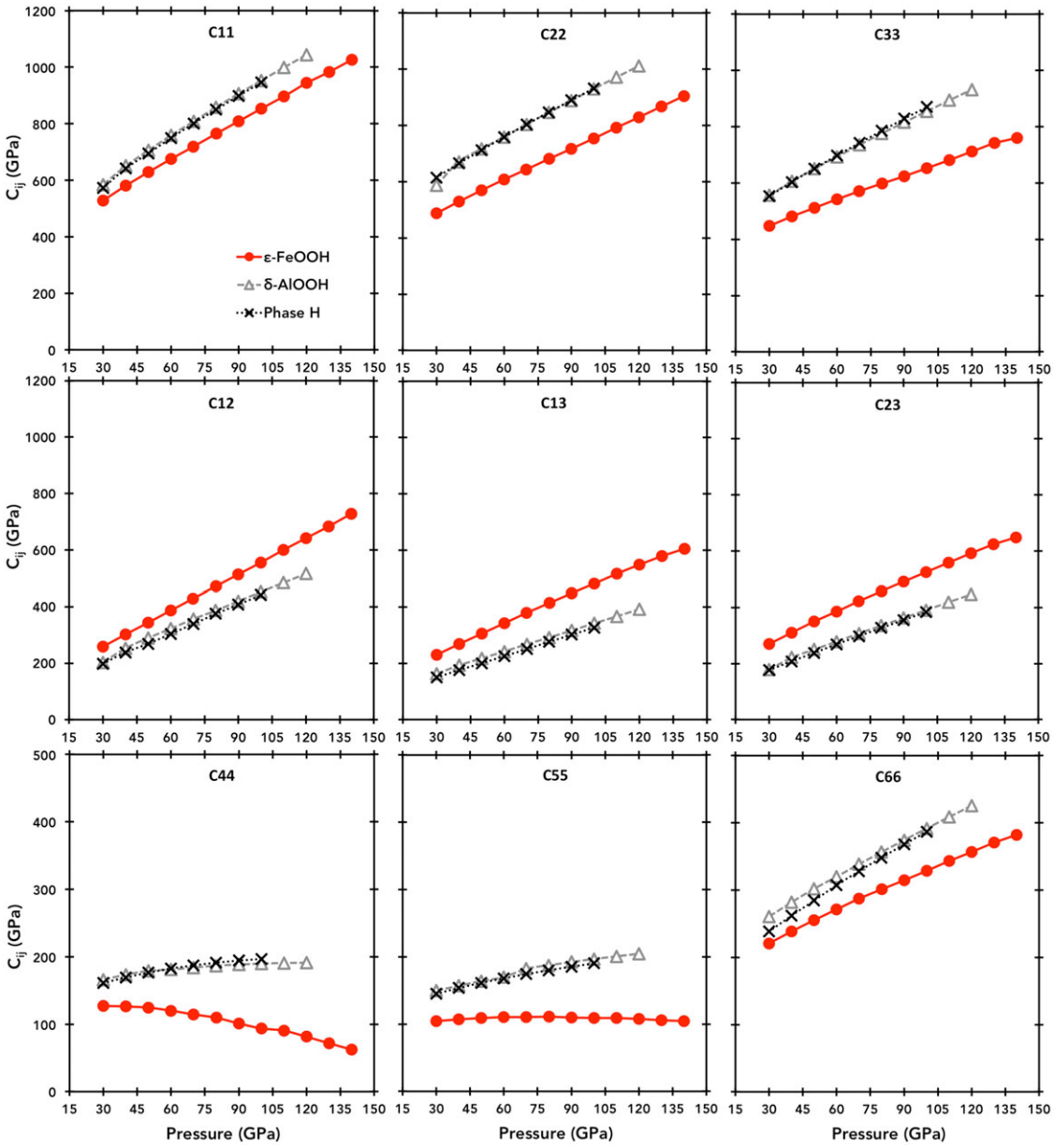

Figure 3. Elastic constants of low-spin ferromagnetic ε-FeOOH calculated with self-consistent U parameter (filled circles, this study), δ-AlOOH (open triangles) [*Tsuchiya and Tsuchiya*, 2009], and phase H (open cross symbols) [*Tsuchiya and Mookherjee*, 2015] between 30 and 140 GPa.

more gradual pressure-dependent evolution in the structure of the density of state above 20 GPa and independent of hydrogen bond symmetrization. The general structure of the density of state and band gap width at 60 GPa are similar to those calculated for ferromagnetic low-spin ε-FeOOH at comparable pressure by *Otte et al.* [2009].

3.3. Elastic Constants

The elastic tensor of the high-pressure hydrogen-centered structure of ε-FeOOH was determined up to CMB pressure. Because of the orthorhombic symmetry of ε-FeOOH, there are nine unique elastic constants needed to fully describe the elastic behavior of this phase as a function of pressure (Figure 3). Calculated structures using only GGA, without the addition of the columbic self-interaction term (*U*) are systematically smaller than structures determined using the GGA + *U* method at the same pressure. Yet a comparison of GGA and GGA + *U* elastic constants, normalized by volume, reveals little discrepancy (mean deviation <8%) in the value or trend of the elastic constants of the HC structure over the

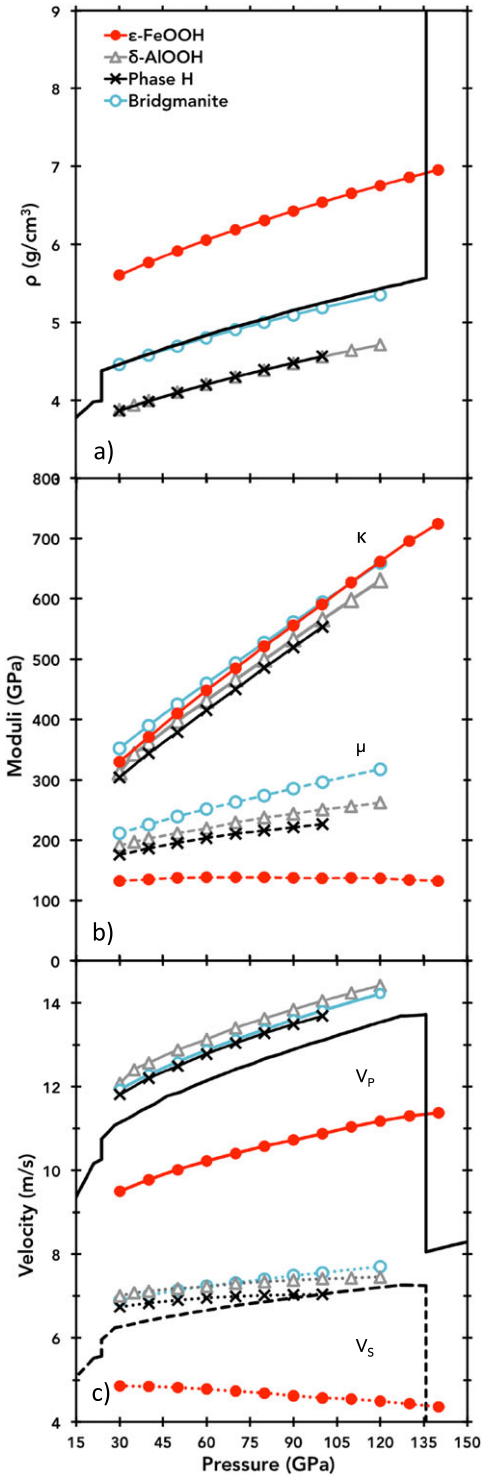

Figure 4. Comparison of the elastic properties of ε-FeOOH, δ-AlOOH, phase H, and $MgSiO_3$ bridgmanite as a function of pressure, including (a) density, (b) bulk moduli (solid lines) and shear moduli (dashed lines), and (c) aggregate compressional (solid lines) and shear wave velocities (dotted lines). All values plotted are 0 K values excluding those of PREM. Phase H and δ-AlOOH literature data are from *Tsuchiya and Mookherjee* [2015] and *Tsuchiya and Tsuchiya* [2009], respectively, and bridgmanite data are from *Wentzcovitch et al*. [2004].

pressure range investigated. Seven of the nine elastic constants exhibit positive slopes and smooth trends indicative of gradual stiffening with increasing pressure, while the C_{55} elastic constant is pressure insensitive and the C_{44} elastic constant decreases with increasing pressure. The three Born stability criteria [*Born and Huang*, 1954] relevant to orthorhombic symmetry (Text S1) were calculated for the entirety of the pressure range for which the HC structure elastic constants were determined (30 to 140 GPa), and the structure was found to be mechanically stable, as shown in Figure S3. Nevertheless, the negative pressure dependence of C_{44} is indicative of eventual mechanical instability at sufficiently high pressures. To better constrain the elastic behavior of intermediate compositions, the elastic tensor of ε-FeOOH is compared to that of δ-AlOOH and phase H, with which it is isostructural. The Fe-end-member (ε-FeOOH) has smaller diagonal elastic constants and larger off-diagonal elastic constants than those of either δ-AlOOH [*Tsuchiya and Tsuchiya*, 2009] or phase H [*Tsuchiya and Mookherjee*, 2015] (Figure 3).

Bulk and shear moduli of the HC phase were calculated from single crystal elastic constants using the Voigt-Reuss-Hill averaging scheme as shown in Figure 4 and Table 3 [*Hill*, 1952]. The bulk modulus (K) of HC-structure ε-FeOOH smoothly increases with pressure, but the shear modulus (μ) is nearly pressure independent. In comparison with that of ε-FeOOH, the bulk modulus and its pressure dependence of both phase H and hydrogen-centered structure of δ-AlOOH are quite similar, averaging 7% and 10% lower, respectively, across the 30 to 100 GPa pressure interval [*Tsuchiya and Mookherjee*, 2015; *Tsuchiya and Tsuchiya*, 2009]. The pressure

Table 3. Density, Hill Averages of Bulk Moduli (K), Shear Moduli (μ), and Sound Velocities at 60 and 90 GPa for ε-FeOOH (This Study), δ-AlOOH [*Tsuchiya and Tsuchiya*, 2009], and Phase H [*Tsuchiya et al*., 2015]

	ε-FeOOH		δ-AlOOH		Phase H	
P (GPa)	60	90	60	90	60	90
ρ (g/cm^3)	6.055	6.428	4.204	4.476	4.202	4.481
K (GPa)	448.2	556.2	431.7	532.3	415.0	519.6
μ (GPa)	138.3	137.4	219.7	243.8	203.4	221.6
V_S (km/s)	4.78	4.62	7.23	7.38	6.99	7.11
V_P (km/s)	10.22	10.73	13.13	13.84	12.82	13.56
V_ϕ (km/s)	8.60	9.30	10.13	10.91	9.97	10.79

dependence of the shear modulus of ε-FeOOH differs dramatically from those of phase H and δ-AlOOH. Both δ-AlOOH and phase H have positive, albeit small, pressure dependences in contrast to the negative pressure dependence of the Fe-end-member [*Tsuchiya and Mookherjee*, 2015; *Tsuchiya and Tsuchiya*, 2009].

3.4. Sound Velocities

Elastic moduli were used to calculate the aggregate compressional velocity (V_P), shear velocity (V_S), and bulk sound speed (V_ϕ) of ε-FeOOH as a function of pressure (Figure 4c; Table 3). The compressional sound velocity of HC-structure ε-FeOOH increases monotonically with pressure, while the shear velocity gradually decreases with increasing pressure. Similarly, the compressional wave velocity of both phase H and δ-AlOOH show strikingly similar pressure dependences, although the average V_P are ~25 and ~27% higher, respectively, than that of ε-FeOOH across the same pressure interval. However, the pressure dependence of the shear wave velocity of ε-FeOOH differs dramatically from those of phase H and δ-AlOOH, despite cation substitution being the only difference between these phases. Both δ-AlOOH and phase H have positive, although slight, pressure-dependences in in contrast to the negative pressure dependence of the Fe-end-member [*Tsuchiya and Mookherjee*, 2015; *Tsuchiya and Tsuchiya*, 2009]. Due to the paired positive pressure dependence of the compressional velocity and negative pressure dependence of the shear wave velocity, the existence of iron-enriched solid solutions from this system may contribute to previously unexplained large low-shear velocity provinces [*Ganero and McNamara*, 2008].

In addition to aggregate seismic velocities, the single crystal azimuthal anisotropy for compressional waves (AV_P) and the shear wave polarization anisotropy (AV_S) were determined for ε-FeOOH as a function of pressure using the formalism of *Mainprice* [1990], such that

$$AV_P = \frac{V_{P\,\max} - V_{P\,\min}}{\langle V_P \rangle} \times 100$$

$$AV_S = \frac{V_{S\,\max} - V_{S\,\min}}{\langle V_S \rangle} \times 100$$

As shown in Figure 5, ε-FeOOH exhibits substantial shear wave polarization anisotropy that increases with increasing pressure. The degree of shear wave anisotropy in the iron end-member (ε-FeOOH) is similar to, although higher, than previously reported values for phase H and δ-AlOOH [*Tsuchiya and Mookherjee*, 2015] (Figure 5a). The single crystal shear wave anisotropy of ε-FeOOH is horizontally polarized; i.e., the horizontally polarized shear waves (S_H) are larger than vertically polarized shear wave (S_V). This $S_H > S_V$ anisotropy occurs in ε-FeOOH along both *a* and *b* axes, enabling significant shear wave polarization regardless of rotation along the *c* axis (Figure 5b). As such, this significant shear wave polarization would be geophysically significant in conjunction with lattice-preferred orientation (LPO), with considerable flexibility in requisite fabric strength. The existence of iron-rich solid solutions from the FeOOH–AlOOH–$MgSiH_2O_4$ system at the base of the lower mantle could contribute to the $S_H > S_V$ polarization which is seismically observed in that region [*Karato*, 1998]. If seismic anisotropy at the base of the mantle is due to LPO in this system, neither partial melting [e.g., *Williams and Garnero*, 1996] nor sustained high strains needed to maintain anisotropy from shape-preferred orientation (SPO) would need to be invoked to explain the observed seismic phenomena.

4. Geophysical Implications

Increasingly advanced seismic observations, particularly recent tomographic work, have provided evidence that the Earth's mantle is far more heterogeneous than previously believed [e.g., *Lekic et al*., 2012]. Among

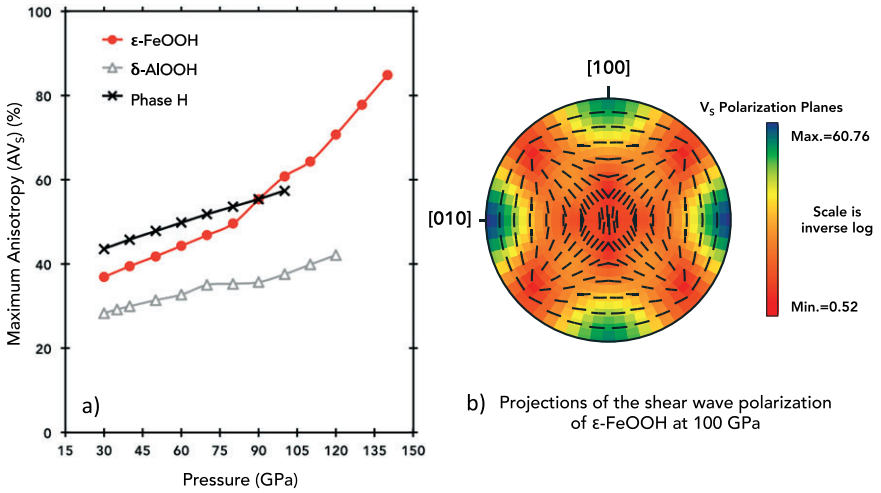

Figure 5. (a) Comparison of the shear wave polarization anisotropy (AV_S) of ε-FeOOH, δ-AlOOH, and phase H as a function of pressure and phase H as a function of pressure. (b) Lambert equal-area upper hemisphere projection of the shear wave polarization (AV_S) of ε-FeOOH generated using software by *Mainprice* [1990].

the observed heterogeneities are pair of continent-scale regions in the Earth's mantle, thousands of kilometers across and likely hundreds of kilometers high, which are seismically distinct from the surrounding mantle material [*Ganero and McNamara*, 2008]. These regions, dubbed large low-shear velocity provinces (LLSVPs), are detectable by their increased density and decreased shear wave velocities and are sharply defined—implying a geochemical rather than solely thermodynamic origin. Since their observation, several potential explanations have been proposed including thermal plumes [*Thompson and Tackley*, 1998], iron-rich melts [*Zhang et al*., 2016], and variable oxidation [e.g., *Gu et al*., 2016], but additional mineral physics investigations are needed to evaluate the stability and material properties of candidate materials at lower mantle conditions to find a robust answer to this mystery.

As the most abundant mineral of the lower mantle, bridgmanite ($MgSiO_3$-perovskite) is thought to largely dictate the material properties of this expansive region of the Earth. Although the thermoelastic properties of the FeOOH–AlOOH–$MgSiH_2O_4$ solid solution have yet to be evaluated, the properties of volumetrically dominant bridgmanite have been calculated [*Wentzcovitch et al*., 2004] allowing for the comparison of 0 K ε-FeOOH material properties with the material properties of 0 K bridgmanite, with the assumption that observed differences scale proportionally with temperature. As shown in Figure 4c, the compressional and shear wave velocities of δ-AlOOH and $MgSiH_2O_4$ do not dramatically differ from that of bridgmanite, but the velocities of ε-FeOOH do. Specifically, the V_P of ε-FeOOH is reduced compared to bridgmanite by a near-constant margin (21.0 ± 0.5%), while the V_S deviates progressively from an initial reduction of ~29.6% at 30 GPa to a reduction of ~43.5% by CMB pressure. Due to this pronounced difference, less than 1 vol % of FeOOH is needed in order to reproduce the ~0.27% V_S reduction characteristic of LLSVPs [*Ganero et al*., 2016]. Future high-temperature experiments and molecular dynamics calculations could aid in assessing the validity of the necessary assumption that elastic properties scale consistently with temperature across phases.

In the evaluated ternary FeOOH–AlOOH–$MgSiH_2O_4$ system, ε-FeOOH is anomalous in the negative pressure-dependent behavior of its shear velocity. The addition of similar vol % amount of δ-AlOOH or $MgSiH_2O_4$ has little impact on the V_S of bridgmanite. While it is unlikely that large regions of end-member ε-FeOOH exist in the deep Earth, regions of iron-enriched, hydrated rock assemblages may be prevalent. And since only small vol % of FeOOH are needed to mimic the shear wave velocity reductions of LLSVPs, it is plausible that iron-enriched solid solutions from the FeOOH–AlOOH–$MgSiH_2O_4$ system contribute to the observed seismic properties of large low-shear velocity provinces in the Earth's lower mantle. These intermediate compositions would bear a seismic signature similar to that of LLSVPs, and the thermodynamic (i.e., *P-T*) stability of the phases are likely enhanced by the addition of aluminum, which has been experimentally shown to substantially increase the stability of phase H [*Nishi et al*., 2017; *Ohira et al*., 2014; *Panero and Caracas*, 2017].

Additionally, the horizontally polarized shear wave anisotropy of ε-FeOOH implies that iron-rich solid solutions from the FeOOH–AlOOH–$MgSiH_2O_4$ system, exhibiting LPO in which the *c* axis is vertically aligned due to the strong shear stresses at the CMB, could contribute to the seismically observed $S_H > S_V$ polarization at the base of the mantle [*Karato*, 1998].

5. Conclusions

We have investigated the structural properties of low-spin ε-FeOOH up to core-mantle boundary pressure. An abrupt change in the structural parameters of ε-FeOOH at 10–20 GPa indicates a second-order phase transition due to pressure-induced hydrogen bond symmetrization. While the calculated pressure of hydrogen bond symmetrization occurs below prevailing estimates of the stability of the low-spin phase, it is important to nevertheless study the influence that hydrogen-bond symmetrization has on the bulk properties of minerals. These findings are in contrast to those of *Gleason et al*. [2013], who report a hydrogen bond symmetrization coincident with the high → low spin transition. Rather, it is our finding that hydrogen bonds of ε-FeOOH are symmetrized tens of GPa in advance of this spin transition. In this case hydrogen bond symmetrization corresponded to a change in the equation of state of the bulk material, a change in the elastic behavior, and a change in the electronic density of states. Determining the high-pressure properties of hydrous phases such as ε-FeOOH is a critical step to future studies of more complex systems. Additionally, systematically describing the influence of proton behavior on seismic observables such as density and sound speeds may allow us to better constrain the quantity and location of water in the lower mantle.

The elasticity of the hydrogen-bond symmetric low-spin ferromagnetic ε-FeOOH was determined from stress-strain relations up to core-mantle boundary pressure. The bulk (K) and shear (μ) moduli, and sound velocities (V_P, V_S) of the HC phase were calculated from these elastic constants and compared against those of the Preliminary Reference Earth Model (PREM) and 0 K bridgmanite. In comparison to different compositions with which it is isostructural and likely to form a solid solution (i.e., phase H and δ-AlOOH), ε-FeOOH is anomalous in regard to the negative pressure dependence of its shear wave velocity. Using bridgmanite as a well-studied proxy for the sound velocities of the bulk lower mantle, it was determined that FeOOH–AlOOH–$MgSiH_2O_4$ solid solutions containing between 0.6 and 0.9 vol % ε-FeOOH would reproduce the observed reduced shear wave velocities characteristic of large low-shear velocity provinces. And because ε-FeOOH exhibits significantly shear wave polarization anisotropy, these same iron-rich solid solutions could also help explain the seismically observed $S_H > S_V$ anisotropy in this region of the deep Earth [*Karato*, 1998].

Acknowledgments

The authors declare no real or perceived financial conflicts of interest related to this work. Supporting information can be found in the supplemental documents. This work was supported by a National Science Foundation Graduate Research Fellowship under grant DGE-1144082 and EAPSI Program grant SP-1612833, jointly funded through the U.S. National Science Foundation and the Japan Society for the Promotion of Science (JSPS) for E.T. This study was supported in part by NSF grant EAR-1427123 for A.C. This study was also partly supported by JSPS KAKENHI grants JP26400516, JP26287137, and JP15H05834 for J.T.

References

Bendeliani, N. A., M. I. Baneyeva, and D. S. Poryvkin (1972), Synthesis of a new modification of FeO(OH) stable at high pressures, *Geokhimiya*, *7*, 871–873, doi:10.2138/am.2014.4994. AN: 020182293.

Bindi, L., M. Nishi, J. Tsuchiya, and T. Irifune (2014) Crystal chemistry of dense hydrous magnesium silicates: The structure of phase H, $MgSiH_2O_4$, synthesized at 45 GPa and 1000°C, *Am. Mineral.*, *99*, 1802–1805, doi:10.2138/am.2014.4994.

Bindi, L., M. Nishi, and T. Irifune (2015), Partition of Al between phase D and phase H at high pressure: Results from a simultaneous structure refinement of the two phases coexisting in a unique grain, *Am. Mineral.*, *100*, 1637–1640, doi:10.2138/am-2015-5327.

Birch, F. (1947), Finite Elastic Strain of Cubic Crystals, *Phys. Rev.*, *71*, 809, doi:10.1103/PhysRev.71.809.

Bolotina, N. B., V. N. Molchanov, T. I. Dyuzheva, L. M. Lityagina, and N. A. Bendeliani (2008), Single-crystal structures of high-pressure phases FeOOH, FeOOD, and GaOOH, *Crystallogr. Rep.*, *53*, 960, doi:10.1134/S1063774508060084.

Born, M., Huang, K. 1954. *Dynamical Theory of Crystal Lattices*. Oxford Univ. Press, London, U.K. doi:10.1119/1.1934059.

Cococcioni, M., and S. de Gironcoli (2005), Linear response approach to the calculation of the effective interaction parameters in the LDA+U method, *Phys. Rev. B*, *71*, 035105, doi:10.1103/PhysRevB.71.035105.

Ganero, E. J., and A. K. McNamara (2008), Structure and dynamics of Earth's lower mantle, *Science*, *320*, 626, doi:10.1126/science.1148028.

Ganero, E. J., A. K. McNamara, and S.-H. Shim (2016), Continent-sized anomalous zones with low seismic velocity at the base of the Earth's mantle, *Nat. Geosci.*, *9*, 481–489, doi:10.1038/ngeo2733.

Giannozzi, P., et al. (2009), Quantum ESPRESSO: A modular and open-source software project for quantum simulations of materials, *J. Phys. Condens. Matter*, *21*, 395502, doi:10.1088/0953-8984/21/39/395502.

Gleason, A. E., R. Jeanloz, and M. Kunz (2008), Pressure-temperature stability studies of FeOOH using X-ray diffraction, *Am. Mineral.*, *93*, 11–12, doi:10.2138/am.2008.2942.

Gleason, A. E., C. E. Quiroga, A. Suzuki, R. Pentcheva, and W. L. Mao (2013), Symmetrization driven spin transition in ε-FeOOH at high pressure, *Earth Planet. Sci. Lett.*, *379*, 49–55, doi:10.1016/j.epsl.2013.08.012.

Gu, T., M. Li, C. McCammon, and K. K. M. Lee (2016), Redox induced lower mantle density contrast and the effect on mantle structure and primitive oxygen, *Nat. Geosci.*, *9*, 723–728, doi:10.1038/NGEO2772.

Hill, R. (1952), The elastic behavior of a crystalline aggregate, *Proc. Phys. Soc. A*, *65*, 349–354, doi:10.1088/0370-1298/65/5/307.

Hu, Q., D. Y. Kim, W. Yang, L. Yang, Y. Meng, L. Zhang, and H.-K. Mao (2016), FeO_2 and FeOOH under deep lower-mantle conditions and Earth's oxygen-hydrogen cycles, *Nature*, *534*, 241–245, doi:10.1038/nature18018.

Ichikawa, I., T. Tsuchiya, and Y. Tange (2014), The P-V-T equation of state and thermodynamic properties of liquid iron, *J. Geophys. Res. Solid Earth*, *119*, 240–252, doi:10.1002/2013JB010732.
Inoue, T. (1994), Effect of water on melting phase relations and melt composition in the system Mg_2SiO_4-$MgSiO_3$-H_2O up to 15 GPa, *Phys. Earth Planet. Inter.*, *85*, 237–263, doi:10.1016/0031-9201(94)90116-3.
Jang, B. J., D. Y. Kim, and J. H. Shim (2017), Metal-insulator transition and the role of electron correlation in FeO_2, *Phys. Rev. B*, *95*, 075144, doi:10.1103/PhysRevB.95.075144.
Karato, S. (1998), Seismic anisotropy in the deep mantle, boundary layers, and the geometry of mantle convection, *Pure Appl. Geophys.*, *151*, 565–587, doi:10.1007/s000240050130.
Karato, S., M. S. Paterson, and J. D. Fitzgerald (1986), Rheology of synthetic olivine aggregates: Influence of grain-size and water, *J. Geophys. Res.*, *91*, 8151–8176, doi:10.1029/JB091iB08p08151.
Karki, B. B., L. Stixrude, and R. M. Wentzcovitch (2001), High-pressure elastic properties of major materials of Earth's mantle from first principles, *Rev. Geophys.*, *39*, 507–534, doi:10.1029/2000RG000088.
Kuribayashi, T., A. Sano-Furukawa, and T. Nagase (2014), Observation of pressure-induced phase transition of δ-AlOOH by using single crystal synchrotron X-ray diffraction method, *Phys. Chem. Miner.*, *41*, 303–312, doi:10.1007/s00269-013-0649-6.
Lekic, V., S. Cottaar, A. Dziewonski, and B. Romanowicz (2012), Cluster analysis of global lower mantle tomography: A new class of structure and implications for chemical heterogeneity, *Earth Planet. Sci. Lett.*, *357-358*, 68–77, doi:10.1016/j.epsl.2012.09.014.
Mainprice, D. (1990), An efficient FORTRAN program to calculate seismic anisotropy from the lattice preferred orientation of minerals, *Comput. Geosci.*, *16*, 383–393.
Momma, K., and F. Izumi (2008), VESTA: A three-dimensional visualization system for electronic and structural analysis, *J. Appl. Crystallogr.*, *41*, 653–658, doi:10.1107/S0021889808012016.
Monkhorst, H. J., and J. D. Pack (1976), Special points for Brillouin-zone integrations, *Phys. Rev. B*, *13*, 5188–5192, doi:10.1103/PhysRevB.13.5188.
Nishi, M., Y. Kuwayama, J. Tsuchiya, and T. Tsuchiya (2017), The pyrite-type high-pressure form of FeOOH, *Nature*, doi:10.1038/nature22823.
Ohira, I., E. Ohtani, T. Sakai, M. Miyahara, N. Hirao, Y. Ohishi, and M. Nishijima (2014), Stability of a hydrous δ-phase, AlOOH-$MgSiO_2(OH)_2$, and a mechanism for water transport into the base of the lower mantle, *Earth Planet. Sci. Lett.*, *401*, 12–17, doi:10.1016/j.epsl.2014.05.059.
Ohtani, E., Y. Amaike, S. Kamada, T. Sakamaki, and N. Hirao (2014), Stability of hydrous phase H $MgSiO_4H_2$ under lower mantle conditions, *Geophys. Res. Lett.*, *41*, 8283–8287, doi:10.1002/2014GL061690.
Otte, K., R. Pentcheva, W. W. Schmahl, and J. R. Rustad (2009), Pressure-induced structural and electronic transitions in FeOOH from first principles, *Phys. Rev. B-Condens. Matter Mater. Phys.*, *80*, 1–9, doi:10.1103/PhysRevB.80.205116.
Panero, W., and R. Caracas (2017), Stability of phase H in the $MgSiO_4H_2$-AlOOH-SiO_2 system, *Earth Planet. Sci. Lett.*, *463*, 171–177, doi:10.1016/j.epsl.2017.01.033.
Perdew, J. P., K. Burke, and M. Ernzerhof (1996), Generalized gradient approximation made simple, *Phys. Rev. Lett.*, *77*, 3865–3868, doi:10.1103/PhysRevLett.77.386.
Sano, A., E. Ohtani, T. Kondo, N. Hirao, T. Sakai, N. Sata, Y. Ohishi, and T. Kikegawa (2008), Aluminous hydrous mineral δ-AlOOH as a carrier of hydrogen into the core-mantle boundary, *Geophys. Res. Lett.*, *35*, L03303, doi:10.1029/2007GL031718
Sano-Furukawa, A., H. Kagi, T. Nagai, S. Nakano, S. Fukura, D. Ushijim, E. Iizuka, and T. Yagi (2009), Change in compressibility of δ-AlOOD and δ-AlOOH at high pressure: A study of isotope effect and hydrogen-bond symmetrization, *Am. Mineral.*, *94*, 1255–1261, doi:10.2138/am.2009.3109.
Suzuki, A. (2010), High-pressure X-ray diffraction study of ε-FeOOH, *Phys. Chem. Miner.*, *37*, 153–157, doi:10.1007/s00269-009-0319-x.
Thompson, P. F., and P. J. Tackley (1998), Generation of mega-plumes from the core-mantle boundary in compressible mantle with temperature-dependent viscosity, *Geophys. Res. Lett.*, *25*, 1999–2002, doi:10.1029/98GL01228.
Troullier, N., and J. L. Martins (1991), Efficient pseudopotential for plane-wave calculations, *Phys. Rev. B*, *43*, 1993–2006, doi:10.1103/PhysRevB.43.1993.
Tsuchiya, J. (2013), First principles prediction of a new high-pressure phase of dense hydrous magnesium silicates in the lower mantle, *Geophys. Res. Lett.*, *40*, 4570–4573, doi:10.1002/grl.50875.
Tsuchiya, J., and M. Mookherjee (2015), Crystal structure, equation of state, and elasticity of phase H ($MgSiO_4H_2$) at Earth's lower mantle pressures, *Sci. Rep.*, *5*, 15534, doi:10.1038/srep15534.
Tsuchiya, J., and T. Tsuchiya (2009), Elastic properties of δ-AlOOH under pressure: First principles investigation, *Phys. Earth Planet. Inter.*, *174*, 122–127, doi:10.1016/j.pepi.2009.01.008.
Tsuchiya, J., T. Tsuchiya, S. Tsuneyuki, and T. Yamanaka (2002), First principles calculation of a high-pressure hydrous phase δ-AlOOH, *Geophys. Res. Lett.*, *29*(19), 1909, doi:10.1029/2002GL015417.
Tsuchiya, T., R. M. Wentzcovitch, C. R. S. da Silva, and S. de Gironcoli (2006), Spin transition in magnesiowüstite in Earth's lower mantle, *Phys. Rev. Lett.*, *96*, 198501, doi:10.1103/PhysRevLett.96.198501.
Umemoto, K., and R. M. Wentzcovitch (2005), Theoretical study of the isostructural transformation in ice VIII, *Phys. Rev. B*, *71*, doi:10.1103/PhysRevB.71.012102.
Vanderbilt, D. (1990), Soft self-consistent pseudopotentials in a generalized eigenvalue formalism, *Phys. Rev. B*, *41*, 7892–7895, doi:10.1103/PhysRevB.41.7892.
Wang, D., M. Mookherjee, Y. Xu, and S. Karato (2006), The effect of water on the electrical conductivity of olivine, *Nature*, *443*(26), 977–980, doi:10.1038/nature05256.
Wentzcovitch, R. M. (1991), Invariant molecular dynamics approach to structural phase transitions, *Phys. Rev. B*, *44*, 2358–2361, doi:10.1103/PhysRevB.44.2358.
Wentzcovitch, R. M., B. B. Karki, M. Cococcioni, and S. de Gironcoli (2004), Thermoelastic properties of $MgSiO_3$-perovskite: Insights on the nature of the Earth's lower mantle, *Phys. Rev. Lett.*, *92*, 018501–4, doi:10.1103/PhysRevLett.92.057001.
Williams, Q., and E. J. Garnero (1996), Seismic evidence for partial melt at the base of Earth's mantle, *Science*, *273*, 1528–1530, doi:10.1126/science.273.5281.1528.
Xu, W., et al. (2013), Pressure-induced hydrogen bond symmetrization in iron oxyhydroxide, *Phys. Rev. Lett.*, *111*(17), 1–5, doi:10.1103/PhysRevLett.111.175501.
Zhang, Z., S. M. Dorfman, J. Labidi, S. Zhang, M. Li, M. Manga, L. Stixrude, W. F. McDonough, and Q. Williams (2016), Primordial metallic melt in the deep mantle, *Geophys. Res. Lett.*, *43*, 3693–3699, doi:10.1002/2016GL068560.